ORIGINAL ARTICLE

A framework for predicting three-dimensional prostate deformation in real time

Alex Jahya
Mark Herink
Sarthak Misra*

Institute for Biomedical Technology and Technical Medicine (MIRA), University of Twente, The Netherlands

*Correspondence to: S. Misra, Carré 3.609, CE-EWI, PO Box 217, 7500AE Enschede, The Netherlands.
E-mail: s.misra@utwente.nl

Abstract

Background   Surgical simulation systems can be used to estimate soft tissue deformation during pre- and intra-operative planning. Such systems require a model that can accurately predict the deformation in real time. In this study, we present a back-propagation neural network for predicting three-dimensional (3D) deformation of a phantom that incorporates the anatomy of the male pelvic region, i.e. the prostate and surrounding structures that support it.

Method   In the experiments and simulations, a needle guide is used to deform the rectal wall. The neural network predicts the deformation based on the relation between the undeformed and deformed shapes of the phantom. Training data are generated using a validated finite element (FE) model of the prostate and its surrounding structures. The FE model is developed from anatomically accurate magnetic resonance (MR) images. An ultrasound-based acoustic radiation force impulse imaging technique is used to measure *in situ* the shear wave velocity in soft tissue. The velocity is utilized to calculate the elasticities of the phantom. In the simulation study, the displacement and angle of the needle guide are varied. The neural network then predicts 3D phantom deformation for a given input displacement.

Results   The results of the simulation study show that the maximum absolute linear and angular errors of the nodal displacement and orientation between neural network and FE predicted deformation are 0.03 mm and 0.01°, respectively.

Conclusions   This study shows that a back-propagation neural network can be used to predict prostate deformation. Further, it is also demonstrated that a combination of ultrasound data, MR images and a neural network can be used as a framework for accurately predicting 3D prostate deformation in real time. Copyright © 2013 John Wiley & Sons, Ltd.

Keywords   finite element; neural network; surgical simulation system; back-propagation algorithm; prostate; biopsy; real time; needle insertion; ultrasound

Introduction

Surgical simulation systems offer a safe and effective method for training and for pre- and intra-operative planning. Such simulation systems can be used for percutaneous surgeries such as prostate biopsy and brachytherapy. The prostate is located within the pelvic cavity and surrounded by critical structures, such as nerve bundles and blood vessels. Moreover, the volume of the prostate is small (approximately 40 mm × 20 mm × 20 mm) (1). Thus, inexperienced physicians generally require hours of training in order to be competent in performing the percutaneous surgeries. Planning is also essential for preventing misplacement
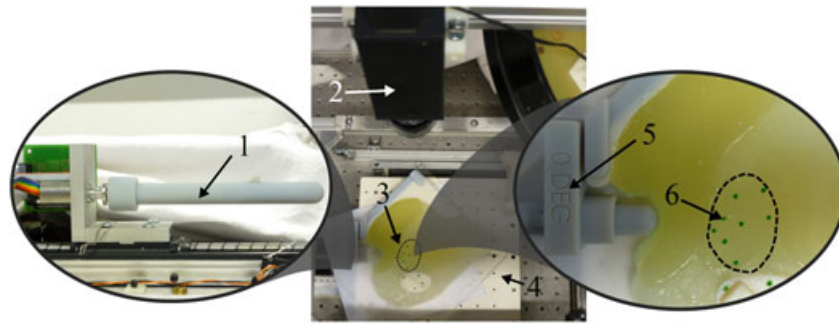
Figure 1. The experimental set-up used to validate the results of the finite element analysis: 1, needle guide; 2, camera; 3, gelatin phantom; 4, experimental table; 5, guide block; 6, markers. Dashed line shows the outline of the prostate.

of the needle tip during the procedure. Errors in needle tip placement result in surgical complications such as tissue trauma or urinary incontinence (2).

Misplacement of the tip can be caused by several reasons. The interactions between surgical instruments and soft tissue during the procedure, physiological processes and patient motion often lead to prostate deformation and, subsequently, to motion of the suspected lesion. An accurate patient-specific biomechanical model can aid physicians by predicting prostate deformation in real time during pre- and intra-operative planning. Usage of such a model will reduce errors in the needle tip placement. Moreover, a model that is able to predict soft tissue deformation in real time can also be utilized as a control input for robotic systems in order to accurately target the suspected lesion (3).

One of the methods used to predict soft tissue deformation is finite element (FE) analysis (4–8). The FE model utilizes knowledge about soft tissue, such as elasticity, organ geometry and boundary conditions. This information can be obtained from *in vivo* measurements in order to accurately predict soft tissue deformation. The drawback of the FE analysis for surgical simulation systems is that it is known to be computationally intensive. Several techniques are available to reduce the computational cost of the FE analysis, e.g. scalable parallel solution algorithm and model reduction technique (9,10). The GPU-based implementation of the FE analysis can also be used to significantly reduce the computational time of the FE analysis (11). Nevertheless, the use of a three-dimensional (3D) FE-based model remains a challenge for accurate and real-time simulation systems.

An alternative method for simulation systems is to use statistical modelling-based techniques. These techniques can be utilized to parametrize the statistical properties of training samples with known deformations, and subsequently to predict soft tissue deformation (12). Davatzikos *et al.* used principal mode of co-variation between anatomy and deformation to estimate the two-dimensional (2D) deformation of simplified ellipsoid shapes (13). A neural network can also be used to analyse and obtain properties of the statistical data. Morooka *et al.* presented the possibility of a neural network for predicting the relation between external force and 3D deformed liver-shape (14). However, in their study, the 3D neural network-predicted liver deformations differ from the results of the FE analysis.

Moreover, Zhong *et al.* showed that a neural network can also be used to predict material deformation based on the theory of conservation of energy (15). In their paper, the potential energy stored in the elastic body is propagated through mass points by the cellular neural network activity. However, this method is not a physics-based approach, since an analogy has to be drawn between the force applied and the equivalent electric energy at the contact point. Previous work by De *et al.* also showed that a radial basis function network can be used to reconstruct the deformation fields of a human stomach and a Penrose drain model (16). However, their training data for the neural network was generated using a non-validated FE model. Further, a neural network has also been used to simulate the interaction forces between tool and tissue, i.e. cutting or haptic force feedback (17–19).

In this paper, we demonstrate that a back-propagation neural network can accurately predict the 3D deformed shape of a prostate phantom with both anatomical details and material properties of the prostate and its surrounding structures. The neural network is used to estimate the relationship between the undeformed and deformed shapes of the phantom. The phantom is developed from a series of anatomically accurate magnetic resonance (MR) images of the prostate and its surrounding structures. Further, the FE model is validated with experimental results (Figure 1). The FE model is populated with linear elastic material properties that are estimated based on the shear wave velocity in the phantom. The velocity is measured *in situ* using an ultrasound-based acoustic radiation force impulse (ARFI) imaging technique (20). Subsequently, the validated FE model is used to generate training data for the neural network. Previous work by Misra *et al.* presented that the deformation response of soft tissue when subjected to displacement is dominated by its geometry and boundary conditions, rather than its properties (8). Further, the experimental study performed by Op den Buijs *et al.* showed that a linear elastic FE model can be used to predict target displacements under various loading and boundary conditions (21). Hence, a linear elastic FE model with geometrical non-linearity is used in this study to predict soft tissue deformation.

In comparison to previous studies, we demonstrate that a combination of known medical imaging modalities (ultrasound data and MR images) and a neural network
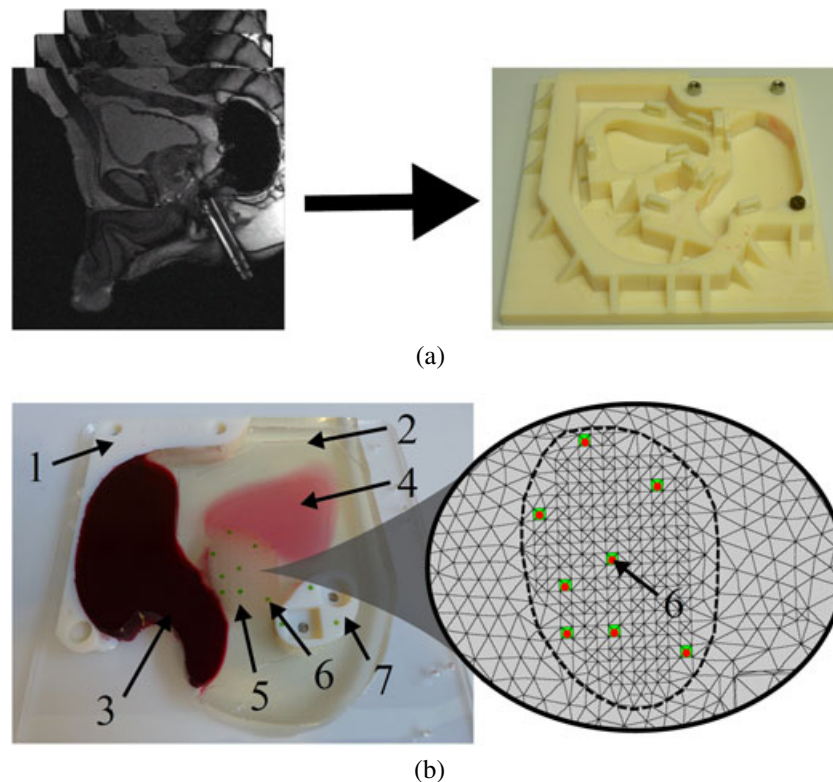
(a)

(b)

Figure 2. (a) Anatomically accurate magnetic resonance images are used to develop a sequential mould (right). (b) The phantom that incorporates the anatomy of the male pelvic region, i.e. the prostate and surrounding structures that support it. The phantom is fabricated using the sequential mould shown in (a). In (b), the anatomy of the male pelvic region incorporated in the phantom are coloured for clarity: 1, spine; 2, adipose tissue; 3, rectal wall; 4, urinary bladder; 5, prostate; 6, markers; 7, pubic bone. Further, inset in (b) presents the finite element model of the prostate and surrounding adipose tissue. Dashed line shows the outline of the prostate, and red dots represent the nodes whose locations correspond to the positions of the marker centroids in the phantom. Markers are shown by green squares.

can be used as a framework to develop accurate surgical simulation of the MR-guided prostate biopsy procedure. Training data for the neural network is generated using a validated FE model that incorporates both the prostate and surrounding structures that support it. Moreover, the results of this study also show that a back-propagation neural network can predict the 3D deformation of a phantom with both anatomical details and material properties of the prostate and its surrounding structures.

In this study, a needle guide is utilized to deform the phantom. Such a guide is routinely used prior to needle insertion during the transrectal MR-guided biopsy procedure. Previous work has shown that needle insertion causes prostate deformation (4,7). De Silva *et al.* showed that lateral tissue motion due to needle insertion is up to 1.5 mm (22). The usage of a needle guide also results in movement and deformation of the prostate (23,24). In our recent work, it is noted that a needle guide can deform the prostate up to 6 mm, or 10% of the longest length of the undeformed prostate (25). Previous work by Karnik *et al.* showed that the needle tip has to be positioned within a spherical radius of 2.5 mm from the suspected lesion for a conclusive biopsy (26). Since the needle guide significantly deforms the prostate during the procedure, this study aims model the deformation for accurate surgical simulation systems.

This paper is organized as follows: the experimental set-up, FE analysis and theory of back-propagation neural network are presented in Section 2. Section 3 discusses the results of the simulation study. Section 4 concludes with a discussion and directions for future work.

Materials and methods

First, details of the experimental set-up are presented. Subsequently, the FE model, and contact and boundary conditions used in the FE analysis are described. Finally, the theory of a back-propagation neural network is explained.

Experimental set-up

Figure 1 presents the experimental set-up, consisting of a one degree-of-freedom (DOF) translational device and a needle guide (item 1). In the experiments, the guide is displaced along its axis using a Misumi translation stage (Misumi Group Inc., Tokyo, Japan) and a Maxon Motor (Maxon Motor AG, Sachseln, Switzerland) (27). An Elmo Whistle 2.5/60 Digital Servo Drive (Elmo Motion Control Ltd, Petach-Tikva, Israel) controls the motor (28). The set-up is used to deform a phantom that incorporates the anatomy of the male pelvic region, i.e. prostate and surrounding structures that support it.

The 3D model of the phantom is developed from a series of anatomically accurate MR images (Figure 2a, left), and using a commercial software ScanIP (Simpleware,
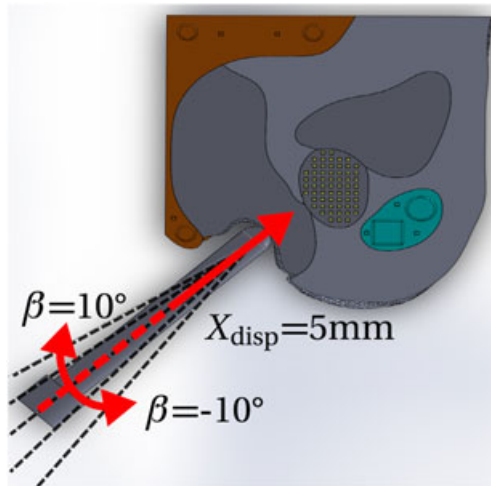
Figure 3. In the experiments and simulations, displacement (X_{disp}) and the angle (β) of the needle guide are varied. For all experiments, the maximum displacement of the guide is 5 mm. Further, β is varied from $-10°$ to $10°$ with a resolution of $5°$. Five experimental cases are used to validate the finite element model. The direction and angle of the displacement of the guide are shown by red arrows.

Table 1. Elasticities of the prostate and its surrounding tissue

Tissue	E_L (kPa)	E_{exp} (kPa)
Adipose tissue (fat)	10.24	10.63
Rectal wall	191.72	172.61
Prostate	60.50	65.89
Urinary bladder	96.87	100.38
Spine and pubic bone	1.82×10^6	2.50×10^3

E_L represents the elasticities of various soft tissue obtained from the literature (8,35,36). E_{exp} is calculated using equation (1). Shear wave velocity in the phantom is measured using the ultrasound-based acoustic radiation force impulse imaging technique. For the spine and pubic bone, E_{exp} is the elasticity of Verowhite–Fullcure830.

Exeter, UK). Subsequently, a sequential mould (Figure 2a, right) is designed to fabricate the phantom (Figure 2b), using SolidWorks 3D computer-aided design (CAD) software (Dassault Systémes SolidWorks Corp., Concord, USA). The mould is printed using an Objet Eden2503D printer (Objet Geometries, Billerica, USA). In the experiments, the needle guide is pushed against the rectal wall (item 3, Figure 2b) at a translational speed of 1 mm/s and an angle of $-10°$ to $10°$ with a resolution of $5°$ (Figure 3). Further, the maximum displacement of the needle guide is 5 mm. The number of experimental cases used to validate the FE model is 5.

The phantom is made using a gelatin mixture (Dr August Oetker KG, Bielefeld, Germany) and it incorporates the anatomy of the male pelvic region. The anatomy includes the prostate and surrounding structures that support it, i.e. pubic bone, rectal wall, adipose tissue and urinary bladder. The compositional percentage of gelatin in the mixture is varied to produce a phantom with linear elastic and homogeneous material properties. The properties are estimated based on the shear wave velocity in the phantom. This velocity is measured *in situ* using a commercially available implementation of an ARFI imaging technique, known as Virtual Touch™ Quantification, installed on a Siemens AcusonS2000 ultrasound machine (Siemens AG, Erlangen, Germany) (28). The elasticities calculated for the prostate and its surrounding tissue are presented in Table 1. The spine and pubic bone (items 1 and 6, Figure 2b, respectively) are made using VeroWhite-FullCure830 (Objet Geometries).

During the experiments, prostate deformation is tracked with the aid of green markers that are embedded at the surface of the phantom (item 6, Figure 1). A camera is used to track the centroids of these markers. The total number of markers on the prostate is eight. For validation, displacements of the centroids are correlated with the nodal

displacements obtained from FE analysis. The locations of the nodes correspond to the positions of the centroids in the phantom (inset, Figure 2b).

The marker tracking algorithm is based on colour thresholding and blob detection, and developed using the OpenCV library (29). The prostate surface deformation is recorded at 30 frames/s via a Sony XCD-710CR charge-coupled device (CCD) camera (item 2, Figure 1) (Sony, Tokyo, Japan), located 71 mm above the needle guide (item 1, Figure 1). The resolution of the camera is 1024 × 768 pixels. The accuracy of the marker tracking algorithm obtained from an evaluation study is 0.2 mm. The experimental results are used to validate the FE model, which is subsequently utilized to generate training data for the neural network.

Finite element model

Previous work by Misra *et al.* showed that the deformation response of soft tissue when subjected to displacement is dominated by its geometry and boundary conditions, rather than its properties (8). Moreover, Op den Buijs *et al.* presented an experimental study and their results showed that a linear FE model can be used to predict target displacements under various loading and boundary conditions (21). Thus, isotropic and linear elastic material properties are used in the FE analysis to predict 3D deformation of the phantom.

The FE model is developed using anatomically accurate MR images, and populated with elasticities calculated using the shear wave velocity in the phantom. The velocity is measured *in situ* using the implementation of ARFI imaging technique. Young's modulus (E) is related to the shear wave velocity in the phantom (20):

$$E = 2(1 + \mu)\upsilon_s^2 \rho, \quad (1)$$

where υ_s is the shear wave velocity, and ρ is the density of the phantom. In the simulations, μ is assumed to be 0.495 for a nearly incompressible phantom. Mean υ_s for the adipose tissue, prostate, urinary bladder and rectal wall are 1.89, 5.03, 6.08 and 7.59 m/s, respectively. The average density of the phantom is 1008 kg/m³.

The FE analysis is performed using ANSYS (Canonburgh, USA) mechanical software. The FE mesh consists of 10-node tetrahedral elements with a minimum and maximum

element edge length of 0.17 and 2 mm, respectively. A mesh resolution study confirms that the maximum element edge length of 2 mm produces consistent results. A further reduction in the maximum edge length does not result in an improvement in the results of the simulation study (FE model validation). The total number of elements in the FE model is 218,290.

Contact and boundary conditions

The anatomy of the male pelvic region incorporated in the phantom is made using the sequential mould (Figure 2a, right). During the manufacturing process, the phantom is allowed to bond during solidification. Thus, the internal contact between the anatomy incorporated in the phantom is modelled as bonded. Moreover, during experiments, the phantom rests on the experimental table (item 4, Figure 1) and lubricant is applied between the phantom and table. This allows free sliding at the interface and prevents the phantom from rupturing when the needle guide is pushed against it. Hence, the contact between the phantom and table is assumed to be frictionless.

At the beginning of the experiment, the needle guide is positioned using a guide block (item 5, Figure 1), such that the tip of the guide just touches the rectal wall. The needle guide is constrained to move only along its cylindrical axis (Figure 3). In the FE model, translational and rotational constraints are also applied to the spine and pubic bone (items 1 and 7, Figure 2b). In the experiments, both the spine and pubic bone are fixed to the experimental table. The results of FE analysis are validated using experiments and subsequently the FE model is utilized to generate training data for the neural network.

Neural network model

A neural network usually consists of input, hidden and output layers (Figure 4) and it can be used to estimate a function for the given input and output training data (30). The output of the neural network depends on the type of activation functions chosen. One of the algorithms used to train a neural network is the back-propagation algorithm (31). This training process can also be seen as an optimization process of a cost function. The back-propagation algorithm works by modifying the weights of the neural network, such that the sum of the squares for the errors between the desired and estimated outputs of the entire training data set (cost function) is minimized. Further, a gradient descent method is used in the optimization process (32).

The time required to train the neural network depends on the number of input and output neurons, and hidden layers. In this study, the displacement and angle of the needle guide serve as inputs to the neural network. The network is trained to predict nodal displacements of the 3D FE model (218,290 nodes). In order to decrease the number of output neurons, principal component analysis (PCA) is utilized (33). After PCA, the original 218,290 elements of output are reduced to 16 elements. Thus, each of the training data (input–output pair) consists of two and 16
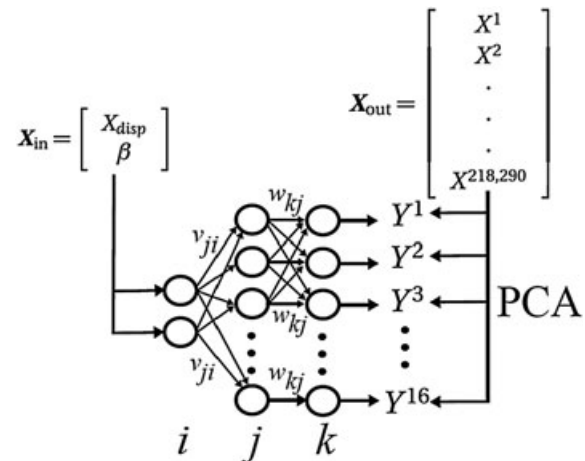
Figure 4. A sketch of the backprogation neural network used in this study. X_{disp} and β are the displacement and angle of the needle guide, respectively, and they serve as the input to the neural network (X_{in}). The network predicts nodal displacements of the 3D FE model (218,290 nodes). Principal component analysis (PCA) is used to decrease the number of output neurons (34). After PCA, the original 218,290 elements of output (X_{out}) are reduced to 16 elements ($Y_1, Y_2, \ldots, Y_{16}$). Thus, each of the training data (input–output pair) consists of two and 16 components of input and output, respectively. i, j, k represent neurons in the input, hidden and output layers, respectively. Further, v_{ji} and w_{kj} represent the weight between input and hidden neurons, and between hidden and output neurons, respectively. In our neural network, the number of hidden layers is 60, and the number of neurons for input and output are 2 and 16, respectively.

components of input and output, respectively. Previous work by Shuxiang *et al.* showed that the optimal number of hidden layers is given by the ratio of the total number of training patterns to the dimensions of the input elements (34). Thus, the total number of hidden layers in our neural network is 60. Subsequently, for a simulation study, the neural network predicts the 3D deformed shape of the phantom for a given input displacement.

Results

This section presents the results of the simulation studies (FE model validation and prostate deformation prediction). First, the discrepancy between the results of experiments and FE analysis (FE model validation) is presented. Then, the errors between the results of neural network-based simulation and FE analysis (prostate deformation prediction) are shown.

Finite element model validation

In order to validate the results of FE analysis with experiments, the centroids of the markers are tracked and their linear and angular displacements are calculated. The total number of markers (item 6, Figure 2b) located on the surface of the prostate is eight. The experimental results are then compared to the nodal linear and angular displacements obtained from FE analysis. The locations of these nodes

Table 2. Results of the validation study between finite element (FE) analysis and experiments

Case	β (°)	e (mm)	σ_e (mm)	θ (°)	σ_θ (°)
1	−10	0.26	0.03	1.33	0.18
2	−5	0.23	0.03	2.81	0.42
3	0	0.16	0.02	4.97	0.24
4	5	0.29	0.05	7.45	1.30
5	10	0.28	0.05	8.62	0.85

The total number of markers on the prostate is eight (item 6, Figure 2b). 'Case' represents the validation cases (Figure 3); for all cases, the maximum displacement of the needle guide is 5 mm. β, angle at which the guide is displaced; e and θ, maximum absolute linear and angular errors of the marker position and orientations, respectively, between the experiments and FE analysis for the eight markers tracked during the experiments; σ_e and σ_θ, mean SD of the linear and angular errors, respectively. The number of experiments is 5. Accuracy of the marker tracking algorithm is 0.2 mm.

correspond to the positions of the centroids in the phantom. Linear and angular errors are calculated as the maximum absolute distance and angle between the results of experiments and FE analysis, respectively. The linear and angular errors for the five validation cases are presented in Table 2. It is seen that the maximum absolute linear error for the marker position between the results of the experiments and FE analysis is 0.29 mm, and it is noted for case 4 (Table 2). On the other hand, the maximum angular error for the marker orientation is 8.62° (case 5).

Prostate deformation prediction

In this study, the neural network is used to predict nodal displacements of the FE model in 3D space. These displacement data for 218,290 nodes of the FE model are regenerated from the 16 components of neural network output by reversing the PCA transformation. The training data for the neural network are generated using the validated 3D FE model. For generating variability in the patterns of the training data, the angle at which the guide deforms the rectal wall is varied from −10° to 10°, with a resolution of 1°. Further, the guide is displaced in steps of 0.25 mm and for a displacement up to 10 mm. Given that the variations in the displacement and angle of the needle guide result in 40 and 21 patterns, respectively, the total number of training data is 840 input–output pairs.

In order to compare the results of neural network-based simulation with FE analysis, we choose the "leave-one-out method" (37). We randomly choose five patterns as test samples and leave these out from the original 840 input–output pairs generated for the training data. This reduces the total number of training data used to train the neural network to 835 input–output pairs. Further, the test samples have different sets of displacement and angles of the needle guide (Table 3) and, hence, they represent distinct initial conditions. The training of the neural network is completed in 38.5 min. Subsequently, for each of the test samples, we compare the nodal displacements predicted by the neural network with the results of FE analysis.

Table 3. The discrepancy between the neural network (NN)- and finite element (FE)-based predictions of 3D phantom deformation

Sample	X_{disp} (mm)	β (°)	e_{NN} (mm)	α (°)	e_r (%)
1	7.75	−5	0.03	0.00	1.02
2	4.25	−3	0.02	0.01	1.01
3	5.25	−2	0.02	0.00	0.83
4	1.5	−1	0.01	0.00	1.40
5	2.5	2	0.01	0.01	1.41

'Sample' represents the test samples. The displacement and angle of the needle guide are represented by X_{disp} and β, respectively; e_{NN} and α, maximum linear and angular errors of the nodal displacement and orientation, respectively, between neural network- and FE-predicted nodal displacements; e_r, maximum relative error (%) of the nodal displacement between the results of the neural network- and FE-based simulation, equation (2).

Linear and angular errors are defined as the maximum absolute distance and angle between the results of neural network-based simulation and FE analysis, respectively. These errors are calculated for the 218,290 nodes of the FE model, and the maximum errors for the five test samples are presented in Table 3. Further, Figure 5 shows the outline of the neural network-predicted prostate deformation overlaid on the corresponding result of the finite element analysis for representative test sample 1 (Table 3). We also calculate relative errors for nodal displacements predicted by the neural network and FE analysis. The relative error (e_r) is given by:

$$e_r = \frac{\|e_i\|}{\max_j \|y_j\|} \times 100\% \text{ with } e_i = y_i - \hat{y}_i \qquad (2)$$

where y_i and $\hat{y}_i$ $\mathbf{R}^{218,290}$ are the 218,290 components of the results of the neural network output after reversing PCA transformation and FE analysis, respectively. The maximum relative errors for the five test samples are also presented in Table 3.

Qualitatively, it can be seen that the neural network is capable of accurately predicting the 3D deformation of the phantom (Figure 5). Quantitatively, it is observed that the maximum absolute linear and angular errors of the nodal displacement and orientation between neural network- and FE-based predictions are 0.03 mm and 0.01°, respectively (Table 3). The mean time taken for the neural network to predict 3D deformation of the phantom for a given input displacement is 0.04 s on a 2.4 GHz Intel i5 computer with 8 GB RAM.

Discussion

Ultrasound and MR images are routinely used for the diagnosis and treatment of prostate cancer. The results of this study show that ultrasound data, MR images and a neural network can be used as a framework to develop accurate surgical simulation of the MR-guided prostate biopsy procedure. In the experiments, the shear wave velocity in the phantom is measured *in situ* using an ultrasound-based ARFI imaging technique. The FE model is developed using anatomically accurate MR images and populated with
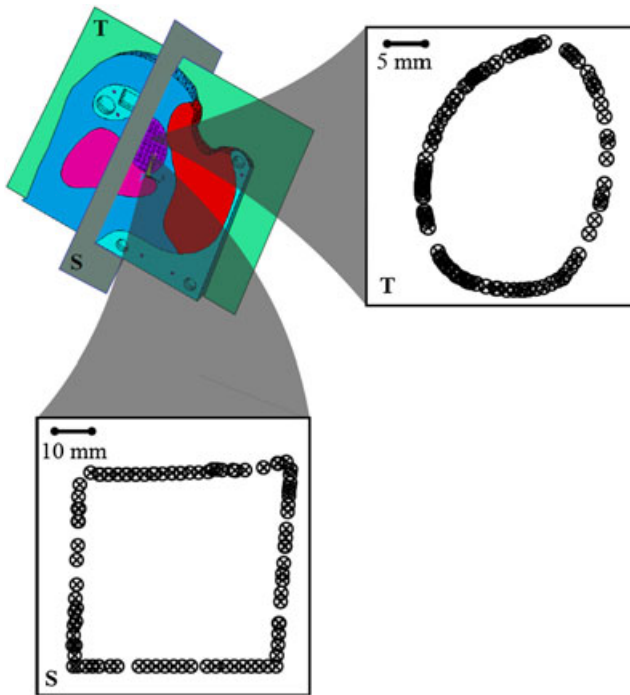
Figure 5. Outline of the neural network-predicted prostate deformation (O) overlaid on the corresponding result of the finite element analysis ($\times$). Outlines of the prostate are taken in both transverse (T) and saggital (S) planes. The outlines are for representative test sample 1, in which the displacement and angle of the needle guide are 7.75 mm and $-5°$, respectively.

elasticities calculated using the shear wave velocity. Subsequently, the training data for the neural network are generated using the linear elastic FE model. The neural network then predicts the 3D deformation of the phantom, based on the statistical properties of the training data. In this study, the FE model is validated with experimental results.

The results of the FE model validation show that a linear elastic FE model can be used to predict soft tissue deformation. The maximum absolute linear and angular errors of the marker position and orientation between the experiments and FE analysis are 0.29 mm and 8.62°, respectively (Table 2). Our results also show that a back-propagation neural network can be used to estimate the principal mode of variation between undeformed and deformed shapes for a given input displacement. Using training samples consisting of 835 patterns of input and output data, the maximum absolute linear and angular errors of the nodal displacement and orientation between neural network- and FE-based predictions are 0.03 mm and 0.01°, respectively (Table 3).

It is noted that the errors between experiments and FE analysis are within the allowable tolerance of the needle tip placement for a conclusive biopsy (26). The FE analysis can be used during surgical preplanning to predict the displacement of the suspected lesion due to prostate deformation. Subsequently, using the predicted location of the lesion, the tip can be accurately positioned within a spherical radius of 2.5 mm from the suspected lesion for an accurate diagnosis during the biopsy procedure. Thus, given that the maximum error in the results of the FE model

validation (0.29 mm) is within the allowable tolerance of tip placement (2.5 mm), the FE model can be used to predict 3D soft tissue deformation.

The discrepancy between the neural network and FE predicted deformation is noted to be significantly small, while the difference between their computational times is significantly large. The mean time taken for the neural network and FE analysis to predict soft tissue deformation is 0.04 s and 11.10 min, respectively. The errors in the neural network-based predictions of suspected lesion displacement are also within the allowable tolerance for a conclusive biopsy. Thus, the proposed neural network can be used as an alternative to FE analysis for accurately predicting 3D soft tissue deformation. Further, the low computational cost of the neural network-based simulation allows real time predictions of soft tissue deformation. Thus, the neural network can be used for accurate surgical simulations systems.

In this study, training data for the neural network are generated using the FE model. The model is validated with experiments based on the surface deformation of the prostate. Nevertheless, the methods presented in this paper can be extended to a validation study based on the volumetric deformation of the prostate. Markers can be positioned in 3D space within the prostate, and MR imaging can be used to track the displacements of the markers.

Conclusion

In this study, we show that a back-propagation neural network can accurately predict 3D deformation of the phantom when it is deformed by the needle guide. The phantom incorporates the anatomy of the male pelvic region, including the prostate and its surrounding tissue. The training data for the neural network are generated using a validated FE model. The results of the FE model validation show that a linear elastic FE model can be used to predict 3D surface deformation of the phantom. The maximum absolute linear and angular errors of the marker position and orientation between the experiments and FE analysis are 0.29 mm and 8.62°, respectively. Moreover, the maximum absolute linear and angular errors of the nodal displacement and orientation between predictions using the neural network and FE analysis are 0.03 mm and 0.01°, respectively. The results of our investigation also demonstrate that a combination of ultrasound data, MR images and a neural network can be used as a framework for real-time 3D simulations of soft tissue deformation.

Future work

During a surgical procedure, physicians insert and manipulate the needle in order to target a suspected lesion. Previous work by De Silva *et al.* showed that needle insertion results in maximum lateral tissue motion of 1.5 mm (22).

Thus, for complete and accurate simulation of the MR-guided prostate biopsy procedure, we will extend the results of our neural network-based simulation study to include needle insertion and for real-time prostate surgical-interventions scenarios. In future work we will also investigate the state-of-the-art techniques for neural network in order to predict prostate deformation due to needle insertion, i.e. pool-based active learning, recurrent, fuzzy and radial basis neural network. Training data for the neural network can be generated using a validated FE model that is able to accurately predict soft tissue deformation, due to both the guide and needle insertion. Further, results of the simulation will also be validated with experiments using soft tissue. MR images can be used to accurately model anatomical details, while the ultrasound-based ARFI imaging technique can be utilized to measure the shear wave velocity in soft tissue for a defined region of interest. Subsequently, the FE model can be populated accordingly with material properties that are estimated based on the shear wave velocity. As part of future work, we will also perform sensitivity studies, where the effects of model uncertainties on prostate deformation response during needle insertion will be investigated. We also plan to combine the proposed neural network with a control algorithm in order to steer the needle tip towards a suspected lesion. The usage of the neural network to predict soft tissue deformation will improve the accuracy of tip placement during the procedure and, hence, the conclusiveness of the diagnosis.

Conflict of Interest

The authors have stated explicitly that there are no conflicts of interest in connection with this article.

Funding

References

1. Benninghoff A. *Anatomie, Makroskopische Anatomie, Embryologie und Histologie des Menschen*, 1st edn. Sinnesorgane, Urban & Schwarzenberg, Munich, 1994.
2. Wust P, von Borczyskowski DW, Henkel T, *et al*. Clinical and physical determinants for toxicity of ^{125}I seed prostate brachytherapy. *Radiother Oncol* 2004; **73**(1): 39–48.
3. Fichtinger G, Fiene JP, Kennedy CW, *et al*. Robotic assistance for ultrasound-guided prostate brachytherapy. *Med Image Anal* 2008; **12**(5): 535–545.
4. Mohamed A, Davatzikos C, Taylor R. A combined statistical and biomechanical model for estimation of intra-operative prostate deformation. In Proceedings of the 5th International Conference on Medical Image Computing and Computer-Assisted Intervention (MICCAI), London, UK, 2002; 2489: 452–460.
5. Alterovitz R, Goldberg K, Pouliot J, *et al*. Registration of MR prostate images with biomechanical modeling and nonlinear parameter estimation. *Med Phys* 2006; **33**(2): 446–454.
6. Crouch JR, Pizer SM, Chaney EL, *et al*. Automated finite-element analysis for deformable registration of prostate images. *IEEE Trans Med Imag* 2007; **26**(10): 1379–1390.
7. Misra S, Ramesh KT, Okamura AM. Modeling of tool–tissue interactions for computer-based surgical simulation: a literature review. *Presence* 2008; **17**(5): 463–491.
8. Misra S, Macura KJ, Ramesh KT, *et al*. The importance of organ geometry and boundary constraints for planning of medical interventions. *Med Eng Phys* 2009; **31**(2): 195–206.
9. Székely G, Brechbühler C, Hutter R, *et al*. Modelling of soft tissue deformation for laparoscopic surgery simulation. In Proceedings of the 1st International Conference on Medical Image Computing and Computer-Assisted Intervention (MICCAI), Cambridge, MA, USA, 1998; 1496: 550–561.
10. Niroomandi S, Alfaro I, Cueto E, *et al*. Real-time deformable models of non-linear tissues by model reduction techniques. *Comput Methods Programs Biomed* 2008; **91**(3): 223–231.
11. Courtecuisse H, Jung H, Allard J, *et al*. GPU-based real-time soft tissue deformation with cutting and haptic feedback. *Progr Biophys Mol Biol* 2010; **103**(2): 159–168.
12. Andresen PR, Bookstein FL, Couradsen K, *et al*. Surface-bounded growth modeling applied to human mandibles. *IEEE Trans Med Imag* 2000; **19**(11): 1053–1063.
13. Davatzikos C, Shen D, Mohamed A, *et al*. A framework for predictive modeling of anatomical deformations. *IEEE Trans Med Imag* 2001; **20**(8): 836–843.
14. Morooka K, Chen X, Kurazume R, *et al*. Real-time nonlinear FEM with neural network for simulating soft organ model deformation. In Proceedings of the 11th International Conference on Medical Image Computing and Computer-Assisted Intervention (MICCAI), New York, USA, 2008; 5242: 742–749.
15. Zhong Y, Shirinzadeh B, Alici G, *et al*. Cellular neural network based deformation simulation with haptic force feedback. In Proceedings of the 9th IEEE International Workshop on Advanced Motion Control (AMC), Istanbul, Turkey, 2006; 380–385.
16. De S, Deo D, Sankaranarayanan G, *et al*. A physics-driven neural networks-based simulation system (PhyNNeSS) for multimodal interactive virtual environments involving nonlinear deformable objects. *Presence* 2011; **20**(4): 289–308.
17. Song W, Yuan K. Haptic modeling for liver cutting based on fuzzy neural network. In Proceedings of the 2005 IEEE/ASME International Conference on Advanced Intelligent Mechatronics (AIM), Monterey, CA, USA, 2005; 1216–1220.
18. Höver R, Kósa G, Székely G, *et al*. Data driven haptic rendering – from viscous fluids to visco-elastic solids. *IEEE Trans Haptics* 2009; **2**(1): 15–27.
19. Kuchenbecker K, Fiene J, Niemeyer G. Improving contact realism through event-based haptic feedback. *IEEE Trans Visualiz Comput Graphics* 2006; **12**(2): 219–230.
20. Palmeri ML, Wang MH, Dahl JJ, *et al*. Quantifying hepatic shear modulus *in vivo* using acoustic radiation force. *Ultrasound Med Biol* 2008; **34**(4): 546–558.
21. Op den Buijs J, Hansen HH, Lopata RG, *et al*. Predicting target displacements using ultrasound elastography and finite element modeling. *IEEE Trans Biomed Eng* 2011; **58**(11): 3143–3155.
22. De Silva T, Fenster A, Bax J, *et al*. Quantification of prostate deformation due to needle insertion during TRUS-guided biopsy: comparison of hand-held and mechanically stabilized systems. *Med Phys* 2011; **38**(3): 1718–1731.
23. Mozer PC, Partin AW, Stoianovici D. Robotic image-guided needle interventions of the prostate. *Rev Urol* 2009; **11**(1): 7–15.
24. Kim Y, Noworolski S, Pouliot J. Analysis of prostate deformation due to different MRI/MRS endorectal coils for image fusion and brachytherapy treatment planning. *Med Phys* 2004; **31**: 1728.
25. Jahya A, Schouten MG, Fütterer JJ, *et al*. On the importance of modelling organ geometry and boundary conditions for predicting three-dimensional prostate deformation. *Comput Methods Biomech Biomed Eng* 2012 (in press). http://dx.doi.org/10.1080/10255842.2012.694876
26. Karnik VV, Fenster A, Bax J, *et al*. Assessment of image registration accuracy in three-dimensional transrectal ultrasound guided prostate biopsy. *Med Phys* 2010; **37**(2): 802–813.
27. Van Veen YRJ, Jahya A, Misra S. Macroscopic and microscopic observations of needle insertion into gels. Proceedings of the

Institute of Mechanical Engineering Part H. *J Eng Med* 2012; **226**: 441–449.

28. Jahya A, Van der Heijden F, Misra S. Observations of three-dimensional needle deflection during insertion into soft tissue. In Proceedings of the 4th IEEE/RAS-EMBS International Conference on Biomedical Robotics and Biomechatronics (BioRob), Rome, Italy, 2012; 1205–1210.

29. OpenCV library: http: //sourcefouge.net/projects/opencvlibrary

30. Igor A, Morton H. *An Introduction to Neural Computing*, 2nd edn. International Thomson Computer Press: London, 1995.

31. Mani G. Learning by gradient descent in function space. In Proceedings of the 1990 IEEE International Conference on Systems, Man and Cybernetics Society (SMCS), CA, USA, 1990; 1–8.

32. Hassoun MH. *Fundamentals of Artificial Neural Networks* (1st edn). MIT Press: Cambridge, MA, 1995.

33. Ilin A, Raiko T. Practical approaches to principal component analysis in the presence of missing values. *J Machine Learning Res* 2010; **11**: 1957–2000.

34. Shuxiang X, Ling C. A novel approach for determining the optimal number of hidden layer neurons for fnn's and its application in data mining. In Proceedings of the 5th International Conference on Information Technology and Applications (ICITA), Queensland, Australia, 2008; 683–686.

35. Hiroshi Y. *Strength of Biological Materials*, 1st edn. Williams and Wilkins: Baltimore, 1970.

36. Comley K, Fleck N. The compressive response of porcine adipose tissue from low to high strain rate. *Int J Impact Eng* 2012; **46**: 1–10.

37. Evgeniou T, Pontil M, Elisseeff A. Leave one out error, stability, and generalization of voting combinations of classifiers. *Machine Learning* 2004; **55**(1): 71–97.